Subcritical bifurcation of a rotating elastic filament in a viscous fluid by the immersed boundary method

Sookkyung Lim *, Charles S. Peskin

Courant Institute of Mathematical Sciences, New York University, 251 Mercer Street, New York, NY 10012, USA

Abstract

A bifurcation occurs when an elastic filament rotates in a viscous fluid at frequency ω (bifurcation parameter). We use the immersed boundary (IB) method to study the interaction between the elastic filament and the surrounding viscous fluid as governed by the incompressible Navier–Stokes equations, and to determine the nature of the bifurcation, which turns out to be subcritical.

Keywords: Immersed boundary method; Bifurcation; Elastic filament; Navier–Stokes equations

1. Introduction

We consider an elastic and neutrally buoyant filament having micro-architecture motivated by bacterial flagella [1] in a fluid of viscosity μ, rotated at one end at frequency ω with the other end free. It is composed of inner and outer layers with motors on the outer layer at the bottom. We assume that the fluid is governed by the Navier–Stokes equations, at a very low but nonzero Reynolds number. The immersed boundary (IB) method [2–4] is used to solve the coupled equations of motion of the filament and the fluid. This numerical method reveals two dynamical motions of the rotating elastic filament depending on the rotation rate ω and also on the initial bend: *twirling*, in which the straight but twisted rod rotates about its centerline, and *overwhirling*, in which the tip of filament "falls down" and rotates around its motor axis in a steady bent state.

In the present paper we study a particular rotation rate $\omega < \omega_c$, where ω_c is the *critical frequency* above which the twirling motion is unstable [5]. For small initial bend, the filament straightens out into a twirling motion, but for large enough initial bend, the bend increases over time and the filament goes into an overwhirling motion.

This *bistability* is characteristic of a subcritical bifurcation [6]. In this respect, our results are contrary to those of [5], where a supercritical bifurcation is claimed.

* Corresponding author. Tel.: +1 (212) 998-3092; Fax: +1 (212) 995-4121; E-mail: limsk@cims.nyu.edu

Computational Fluid and Solid Mechanics 2003
K.J. Bathe (Editor)

2. Equations of motion

We describe the equations of motion in this section. We regard the fluid as incompressible and viscous, and the filament as an elastic structure immersed in this fluid.

$$\mathbf{F}_e = -\frac{\partial E}{\partial \mathbf{X}}, \tag{1}$$

$$\mathbf{F}_{\text{mot}} = c\mathbf{T}_{\text{mot}}, \tag{2}$$

$$\mathbf{F} = \mathbf{F}_e + \mathbf{F}_{\text{mot}}, \tag{3}$$

$$\rho\left(\frac{\partial \mathbf{u}}{\partial t} + (\mathbf{u}\cdot\nabla)\mathbf{u}\right) + \nabla p = \mu\nabla^2\mathbf{u} + \mathbf{f}, \tag{4}$$

$$\nabla\cdot\mathbf{u} = 0, \tag{5}$$

$$\mathbf{f}(\mathbf{x},t) = \int \mathbf{F}(q,r,s,t)\,\delta(\mathbf{x}-\mathbf{X}(q,r,s,t))\,\mathrm{d}q\,\mathrm{d}r\,\mathrm{d}s, \tag{6}$$

$$\frac{\partial \mathbf{X}(q,r,s,t)}{\partial t} = \mathbf{u}(\mathbf{X}(q,r,s,t)) \tag{7}$$

$$= \int \mathbf{u}(\mathbf{x},t)\,\delta(\mathbf{x}-\mathbf{X}(q,r,s,t))\,\mathrm{d}\mathbf{x}. \tag{8}$$

The structure equations (1)–(3) involve several unknown functions of (q,r,s,t), where (q,r,s) are moving curvilinear coordinates and t is the time. These unknown functions are $\mathbf{X}(q,r,s,t)$ which describes the motion of the structure and its configuration at any time, $\mathbf{F}_e(q,r,s,t)$ which is the elastic force density (with respect to $\mathrm{d}q\,\mathrm{d}r\,\mathrm{d}s$) derived from $\mathbf{X}$ in the manner described by Eq. (1) and in more detail below, and $\mathbf{F}_{\text{mot}}(q,r,s,t)$ which is the motor force density

acting in the tangential direction $\mathbf{T}_{\mathrm{mot}}(q,r,s,t)$ near the bottom of the filament only.

In Eq. (1), $\partial E/\partial \mathbf{X}$ is the variational derivative of the elastic energy functional $E[\ ]$. The variational derivative is implicitly defined as follows:

$$\lim_{\epsilon\to 0}\frac{\mathrm{d}}{\mathrm{d}\epsilon}E[\mathbf{X}+\epsilon\mathbf{Y}] = \int \frac{\partial E}{\partial \mathbf{X}}(q,r,s,t)\cdot\mathbf{Y}(q,r,s,t)\,\mathrm{d}q\,\mathrm{d}r\,\mathrm{d}s. \tag{9}$$

The fluid Eqs. (4) and (5) are the Navier–Stokes equations of a viscous incompressible fluid. They involve several unknown functions of $(\mathbf{x},t)$, where $\mathbf{x}=(x_1,x_2,x_3)$ are fixed cartesian coordinates. These unknown functions are the fluid velocity vector $\mathbf{u}(\mathbf{x},t)$, the fluid pressure $p(\mathbf{x},t)$, and the applied force density $\mathbf{f}(\mathbf{x},t)$. The constant parameters ρ and μ in the fluid equations are the fluid density and the fluid viscosity, respectively.

We use the Navier–Stokes equations rather than the Stokes equations even though the Reynolds number is essentially zero and inertial effects are entirely negligible in this application. The nature of our numerical scheme is such that this does no harm (see below).

Finally, the interaction Eqs. (6)–(8) connect the Lagrangian and Eulerian variables. Both equations involve the three-dimensional Dirac delta function

$$\delta(\mathbf{x}) = \delta(x_1)\delta(x_2)\delta(x_3) \tag{10}$$

which expresses the local character of the interaction. The first of the interaction equations describes the relationship between the two corresponding force densities $\mathbf{f}(\mathbf{x},t)\,\mathrm{d}\mathbf{x}$ and $\mathbf{F}(q,r,s,t)\,\mathrm{d}q\,\mathrm{d}r\,\mathrm{d}s$. Eqs. (7) and (8) are the no-slip condition of a viscous fluid, which says that the boundary moves at the local fluid velocity. Each of the interaction equations takes the form of an integral transformation in which the kernel is $\delta(\mathbf{x}-\mathbf{X}(q,r,s,t))$.

3. Numerical method

The equations of motion are solved by the IB method [3]. The algorithm for the numerical solution of Eqs. (1)–(8) will be described in this section.

First, we discuss discretization. Let time proceed in steps of duration Δt, and use a superscript n as the time step index, so that $\mathbf{u}^n$ denotes the whole fluid velocity field at time $t=n\Delta t$, and similarly for all other variables.

The spatial discretization is different for Eulerian (fluid) variables from that of the Lagrangian (structure) variables. For the fluid variables such as $\mathbf{u}$, p, and $\mathbf{f}$, we use a fixed periodic cubic lattice of mesh width h and period m in all three space directions. This lattice, denoted $g_{h,m}$ is formally defined as follows:

$$g_{h,m} = \{\mathbf{x}\colon \mathbf{x}=\mathbf{j}h,\ \mathbf{j}\in\mathcal{Z}_m^3\} \tag{11}$$

where

$$\mathcal{Z}_m = \{0,1,\ldots,m-1\} \tag{12}$$

and arithmetic on $\mathcal{Z}_m$ is understood to be modulo m.

Spatial discretization is based on a discrete elastic structure, i.e., a network of springs. Let the points of this structure be numbered in some arbitrary order $k=1,2,\ldots,K$. Then $\mathbf{X}_k^n$ denotes the position at time step n of the immersed boundary point whose label is k. Similarly, $\mathbf{F}_k^n$ is the force applied to the fluid by that same boundary point, at that time step. Note that $\mathbf{F}_k^n$ is a force, not a force density. Thus

$$\mathbf{F}_k^n \sim \mathbf{F}(q,r,s,n\Delta t)\,\mathrm{d}q\,\mathrm{d}r\ rmds. \tag{13}$$

The elastic part, $(\mathbf{F}_e)_k^n$, of the discrete immersed boundary force can be calculated from the discrete elastic energy $E(\mathbf{X}_1,\ldots,\mathbf{X}_K)$ by differentiation:

$$(\mathbf{F}_e)_k^n = -\frac{\partial E}{\partial \mathbf{X}_k}(\mathbf{X}_1^n,\ldots,\mathbf{X}_K^n). \tag{14}$$

This vector equation is shorthand for

$$(\mathbf{F}_e)_{k\alpha}^n = -\frac{\partial E}{\partial \mathbf{X}_{k\alpha}}(\mathbf{X}_1^n,\ldots,\mathbf{X}_K^n) \tag{15}$$

where $\alpha=1,2,3$ is an index denoting the space direction.

To keep track of the topological structure of the discretized immersed elastic boundary, it is useful to introduce the notion of a link table [2]. Let the elastic links that connect some of the pairs of boundary points (but not all possible pairs!) be numbered in arbitrary order $l=1,2,\ldots,l_{\max}$. Let $k_1(l)$ and $k_2(l)$ be the indices of the points that are connected by link l. (If $k_1(l)$ and $k_2(l)$ are interchanged, it makes no difference.) Then link properties such as stiffness and rest length can be regarded as functions of l, and the elastic forces $((\mathbf{F}_e)_1^n\cdots(\mathbf{F}_e)_k^n)$ can be much more efficiently computed by an algorithm that loops over l than by an algorithm that loops over k.

The elastic energy function that we use in this work is as follows.

$$E(\mathbf{X}^n) = \sum_l \frac{S_0}{2}\left(||\mathbf{X}_{k_1(l)}^n - \mathbf{X}_{k_2(l)}^n|| - L_0(l)\right)^2. \tag{16}$$

Thus each link l represents a linear (Hookean) spring with stiffness S_0 (the same for all links, for simplicity) and rest length $L_0(l)$. We choose a straight filament as equilibrium configuration and set the rest length of each elastic link equal to whatever length that link has in the chosen configuration.

In addition to the elastic force $(\mathbf{F}_e)_k^n$ which is derived from E in the manner described above, we also apply another force $\mathbf{F}_{\mathrm{mot}}$ to the outer layer of the motor part of the filament. Naturally, this force will vanish at all the boundary points except for motor points, where it is given by

$$(\mathbf{F}_{\mathrm{mot}})_k^n = c(\mathbf{T}_{\mathrm{mot}})_k^n \tag{17}$$

where $\mathbf{T}^n_{\text{mot}}$ is the unit tangent vector of the outer layer of the motor part at time step n. Therefore the total force $\mathbf{F}^n$ at time step n is the sum of elastic spring forces and motor forces, i.e.,

$$\mathbf{F}^n_k = (\mathbf{F}_e)^n_k + (\mathbf{F}_{\text{mot}})^n_k. \tag{18}$$

Once the total force $\mathbf{F}^n_k$ is known, the next step of the IB algorithm is to apply these forces to the computational grid of the fluid:

$$\mathbf{f}^n(\mathbf{x}) = \sum_k \mathbf{F}^n_k \delta_h(\mathbf{x} - \mathbf{X}^n_k) \tag{19}$$

where $\mathbf{x} \in g_{h,m}$ and δ_h is a smoothed approximation to the three-dimensional Dirac δ-function.

The next step is to solve the following system of equations for $(\mathbf{u}^{n+1}, p^{n+1})$:

$$\rho\left(\frac{\mathbf{u}^{n+1} - \mathbf{u}^n}{\Delta t} + \sum_{\alpha=1}^{3} u^n_\alpha D^{\pm}_\alpha \mathbf{u}^n\right) + \mathbf{D}^0 p^{n+1} \tag{20}$$

$$= \mu \sum_{\alpha=1}^{3} D^+_\alpha D^-_\alpha \mathbf{u}^{n+1} + \mathbf{f}^n, \tag{21}$$

$$\mathbf{D}^0 \cdot \mathbf{u}^{n+1} = 0. \tag{22}$$

Here, $\mathbf{D}^0$ is the central-difference approximation to ∇ defined by $\mathbf{D}^0 = (D^0_1, D^0_2, D^0_3)$. The forward D^+, the backward D^- and centered D^0 difference operator are defined in the standard way. Thus $\mathbf{D}^0 p$ approximates ∇p and $\mathbf{D}^0 \cdot \mathbf{u}$ approximates $\nabla \cdot \mathbf{u}$. The expression $\sum_{\alpha=1}^{3} D^+_\alpha D^-_\alpha$, which appears in the viscous term, is a difference approximation to the Laplace operator, and the expression $\sum_{\alpha=1}^{3} u_\alpha D^{\pm}_\alpha$, where $u_\alpha D^{\pm}_\alpha$ is an upwind difference approximation to $u_\alpha \partial/\partial \mathbf{X}_\alpha$, is an upwind difference approximation to $\mathbf{u} \cdot \nabla$.

Now we use the Fast Fourier Transform algorithm [7] to solve Eqs. (20)–(22) for the unknowns $(\mathbf{u}^{n+1}, p^{n+1})$. Note that these are linear equations (nonlinear terms involve known quantities at time level n only) with constant coefficients on a periodic domain.

Once $\mathbf{u}^{n+1}(\mathbf{x})$ has been determined, the boundary points are moved at the local fluid velocity in this new velocity field. This is done by the following interpolation scheme:

$$\frac{\mathbf{X}^{n+1}_k - \mathbf{X}^n_k}{\Delta t} = \sum_{\mathbf{x} \in g_{h,m}} \mathbf{u}^{n+1}(\mathbf{x}) \delta_h(\mathbf{x} - \mathbf{X}^n_k) h^3. \tag{23}$$

4. Results, discussion, and conclusions

The results of this paper we all obtained by applying a particular torque to the motor such that the angular frequency of rotation during twirling was $\omega = 17.74\ \text{s}^{-1}$. This frequency was chosen because it is slightly *below* the

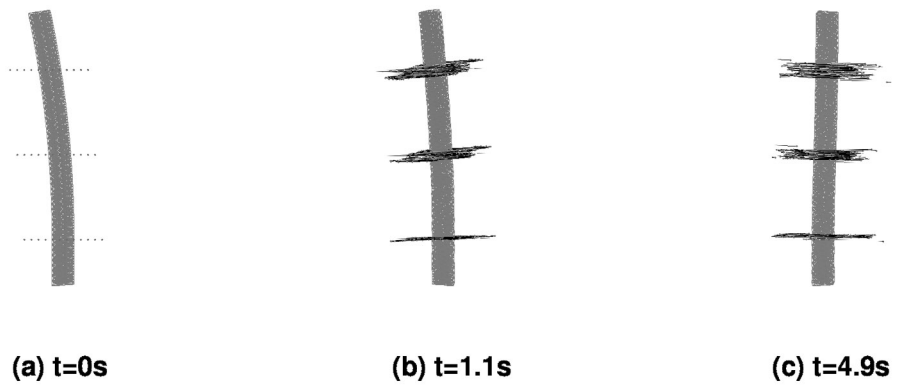

Fig. 1. Twirling motion with small initial bend.

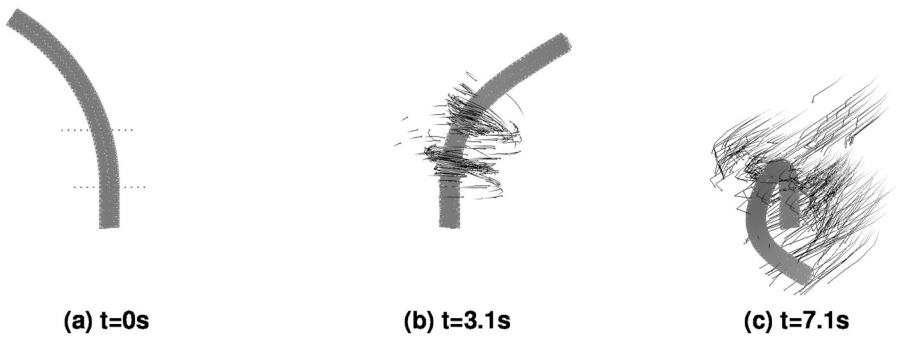

Fig. 2. Overwhirling motion with larger initial bend.

critical frequency found in numerical experiments with the initial condition shown in Fig. 1(a), in which the filament is only slightly bent initially. Thus, at the frequency of our study, the twirling state is linearly stable (stable to small perturbations), but, at a slightly higher frequency, the twirling state is linearly unstable. In other words, we have positioned the bifurcation parameter just *below* the bifurcation frequency.

The linear stability of the twirling state at the chosen frequency is illustrated in Fig. 1, in which a small initial bend relaxes to the twirling state, in which the filament is straight. Fig. 2 reveals, however, that larger initial bend leads to the state we call "overwhirling" in which the overall bend of the filament is more than 180° and the tip "falls down" below the motor. Since all parameters are the same in Figs. 1 and 2, except for the initial conditions, this demonstrates bistability: that the spinning elastic filament in a viscous fluid has two stable dynamical states under the same conditions. Such bistability when the bifurcation parameter is below its critical value is the hallmark of a *subcritical* bifurcation [6]. This result conflicts with [5], in which it is stated that the bifurcation is supercritical.

Acknowledgements

This work was supported by the NIH under research grant R01 GM59875-01A1. Computation was performed at the Applied Mathematics Laboratory, New York University, using immersed boundary software [8] written primarily by Nataniel Cowen, and visualization software [9] written by David McQueen. We thank both Cowen and McQueen not only for the use of their software but also for their kind assistance on many occasions during the course of this research.

References

[1] Jones CJ, Aizawa SI. The bacterial flagellum and flagellar motor: Structure, assembly and function. Adv Microbial Phys 1991;32:109–172.

[2] Peskin CS. Numerical analysis of blood flow in the heart. J Comput Phys 1977;25:220–252.

[3] Peskin CS, McQueen DM. Fluid dynamics of the heart and its valves. In: Othmer HG, Adler FR, Lewis MA, Dallon JC (Eds), Case Studies in Mathematical Modeling: Ecology, Physiology, and Cell Biology. Englewood Cliffs, NJ: Prentice-Hall, 1996, pp. 309–337.

[4] Peskin CS. The immersed boundary method. Acta Numerica 2002;1–39.

[5] Wolgemuth CW, Powers TR, Goldstein RE. Twirling and whirling: Viscous dynamics of rotating elastic filaments. Phys Rev Lett 2000;84:1623.

[6] Strogatz SH. Nonlinear Dynamics and Chaos. Westview Press.

[7] Press WH, Flannery BP, Teukolsky SA, Vetterling WT. Numerical recipes. In: The Art of Scientific Computing. Cambridge University Press, 1986, pp. 390–396.

[8] Cowen NS, McQueen DM, Peskin CS. Immersed Boundary Genereral Software Package (IBGSP), Available by request to peskin@cims.nyu.edu.

[9] McQueen DM. hrtmvp_readmenu_57.f: A Three-Dimensional Visualization Program Using Fortran and SGI GL, Available by request to mcqueen@cims.nyu.edu.